Journal of Saudi Chemical Society (2017) **21**, 180–185

King Saud University

Journal of Saudi Chemical Society

www.ksu.edu.sa
www.sciencedirect.com

ORIGINAL ARTICLE

A facile biosynthesis of copper nanoparticles: A micro-structural and antibacterial activity investigation

Y.T. Prabhu *, K. Venkateswara Rao, V. Sesha Sai, Tambur Pavani

Center for Nano Science and Technology, Institute of Science and Technology, Jawaharlal Nehru Technological University Hyderabad, Hyderabad 500085, India

Received 22 January 2015; revised 7 March 2015; accepted 5 April 2015
Available online 23 April 2015

KEYWORDS

X-ray analysis;
Williamson–Hall plot;
Size-strain plot;
TG/DTA;
Particle analyser;
SEM;
Antibacterial activity

Abstract Nanostructured copper particles are synthesized by *Garcinia mangostana* leaf extract as reducing agent with copper nitrate. X-ray diffraction study confirms the formation of nanocrystalline cubic phase of copper nanoparticles. The micro-structural properties such as grain size, strain, dislocation density and particle size are examined. The lattice constant is calculated using Nelson–Riley function. Physical parameters like lattice constants, stress, strain, dislocation density and size are calculated. Differential thermal analysis (DTA) and thermo gravimetric (TGA) have confirmed that nanoparticles have phase purity and weight loss percentage is 3.328%. The particle size calculated from XRD is 26.51 nm which is in good agreement with the results of W–H plot, SSP methods and particle analyser. The morphology of prepared copper nanoparticles is characterized by scanning electron microscope (SEM) and TEM. These biologically synthesized nanoparticles are highly antibacterial against *Escherichia coli* and *Staphylococcus aureus*.

1. Introduction

Nanostructured materials have been a great attraction for the scientific and technological world in the contemporary times due to their unique properties and applications in various fields [1–3]. In the modern research, preparation and study of nanoparticles is very essential. The optical, electronic, catalytic and magnetic properties are very much dependent on shape, size and chemical surroundings [4–6]. Controlling the shape and size of nanoparticles is very essential in the preparation of nanomaterials. Copper is extensively used because of its physical and chemical properties. In the modern electronic circuits copper (Cu) plays a major role as it is cost efficient [7]. Copper nanoparticles have a long range of applications as super strong materials, antibacterial, sensors and catalysts. Copper nanoparticles react and interact with other particles due to their high surface-to-volume ratio [8].

For the synthesis of Cu nanoparticles many methods were employed in the past such as thermal evaporation [9], chemical synthesis [10], electrochemical synthesis [11], solvothermal

* Corresponding author.
E-mail address: ytprabhusj@gmail.com (Y.T. Prabhu).
Peer review under responsibility of King Saud University.

ELSEVIER Production and hosting by Elsevier

http://dx.doi.org/10.1016/j.jscs.2015.04.002
1319-6103

route [12] and vapour–liquid–solid growth [13]. Green synthesis is cost effective, eco-friendly, no need of high temperatures or pressures and importantly toxic chemicals. It helps to have better progression than chemical and physical methods. Synthesizing nanoparticles using plants is more beneficent than any other biological ways as it would be difficult to maintain the cell cultures. Many other green methods were reported in the synthesis of nanoparticles using plant extracts [14]. Similarly antimicrobial activity using various nanoparticles was also reported [15]. In this paper we report the synthesis of copper nanoparticles from the extract of *Garcinia mangostana* leaf. The structural characterization using XRD and antibacterial activity of biologically synthesized copper nanoparticles were studied.

2. Experiment details

2.1. Plant material and preparation of the extract

Healthy and fresh Garcinia mangosteen leaves were collected and washed with distilled water. Garcinia mangosteen leaves were cut into fine pieces and 25 g of leaves was put in 100 ml of distilled water and boiled for half an hour. The leaf extract was filtered through Whatman No. 1 filter paper. The leaf extract solution was collected. *G. mangostana* leaves are widely used in substitute medicine for the treatment and prevention of tumours. The results obtained with the evaluation of the biological activity of the ethanolic extracts of the fruit, leaves and resin of mangosteen were verified with previous studies regarding their antimicrobial activity. Another observed activity was the potent genotoxic action of the leaf extract, after short exposure of the B16-F10 melanoma cell line. The presence of antimicrobial activity and genotoxic potential in leaves makes further research possible due to the abundance of leaves on the mangosteen tree [16].

2.2. Synthesis of copper nanoparticles

In the synthesis of copper nanoparticles an aqueous solution (0.001 M) of copper nitrate $(CuNO_3)_2$ was used and Garcinia mangosteen leaf extract of 5 ml was added to 95 ml of copper nitrate solution in Erlenmeyer flask. It was heated on water bath at 70 °C for 1 h. It was observed that the colour changes from dark brown to light green indicating the reduction of copper nitrate to copper ions. Thus the copper nanoparticles were obtained. Therefore, the reduction process of metal ions with the formation of nanoparticles is affected by a large number of factors; besides the nature of a plant extract containing active biomolecules in different combinations and concentrations (the effects of which are described above), these include the reaction mixture pH, incubation temperature, reaction time, concentration, and electrochemical potential of a metal ion [17,18]. Due to the limited ability of plants to reduce metal ions, the efficiency of metal nanoparticle synthesis also depends on the electrochemical potential of an ion [35]. Thus, the ability of a plant extract to effectively reduce metal ions may be significantly higher in the case of ions having a large positive electrochemical potential (for example, Ag+) than in the case of ions with a low electrochemical potential such as $([Ag(S_2O_3)_2]^{3-})$ [19]. As discussed above, the proteins that are present in a plant extract may significantly affect the formation of nanoparticles. The approaches that have recently been used for the "green" synthesis of metal nanoparticles combine the use of plant extracts with the exogenous supplementation of the in vitro reactions with biomatrices: peptides, and proteins, whose amino acid sequence and structure are optimized for the efficient production of nanoparticles.

2.3. Antibacterial activity

The antibacterial assays were carried by standard disc diffusion method on *Escherichia coli* (*E. coli*) and *Staphylococcus aureus* (*S. aureus*) which were collected from the stock collection of Centre for Biotechnology, Institute of Science and Technology, Jawaharlal Nehru Technological University Hyderabad, Hyderabad. The culture stocks were revived by inoculating them into freshly prepared sterile nutrient broth and incubated at 37 °C and 110 rpm for 24 h. Once the media got solidified, the bacterial cultures such as *E. coli* and *S. aureus* were smeared and were grown in nutrient broth for 24 h at 37 °C on their respective petriplates.100 µl of the 24 h broth culture of each individual culture was taken. Using sterilized steel cork borer agar wells were made. Each well was filled with 100 µl of different concentrations of copper nanoparticles i.e. 0.20, 0.40, 0.60, 0.80 and 1.0 µg/ml of copper nanoparticles.

2.4. Instrumentation

An X-ray diffractometer (D8 Advance Bruker, Germany) with Cu Kα was used to study the crystallographic phases. Thermal analyses of the samples were done with TG–DTA (EXSTAR TG/DTA6000 series). The surface morphology of Cu nanoparticles was studied using scanning electron microscope (Quanta 400 (FEI)). Particle size analysis was done with particle analyser (HORIBA SZ100).

3. Results and discussion

3.1. XRD

Copper nanoparticles are characterized using XRD. The XRD pattern of copper nanoparticles is shown in Fig. 1 where three

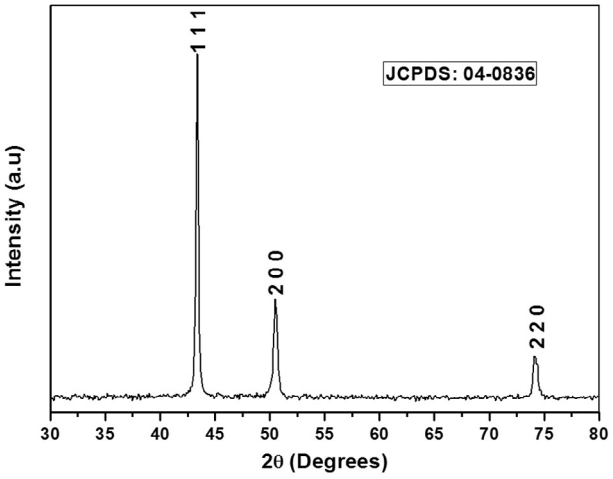

Figure 1 XRD patterns of Cu nanoparticles.

Table 1 Structural parameters of biosynthesized Cu nanoparticles (d – plane spacing, hkl – crystallographic plane, θ – Bragg's angle of diffraction, a – lattice parameter).

Name	d (Å)	hkl	2θ	a_{cal} (Å)	$a_{corrrected}$ (Å)	Av. internal stress $S \times 10^9$ (N/m^2)	Dislocation density ($\rho \times 10^{16}$/m^2)
Cu	2.088	1 1 1	43.37415	3.6097	3.652	0.039	1.42
	1.808	2 0 0	50.50428	3.6099			
	1.278	2 2 0	74.21236	3.6091			

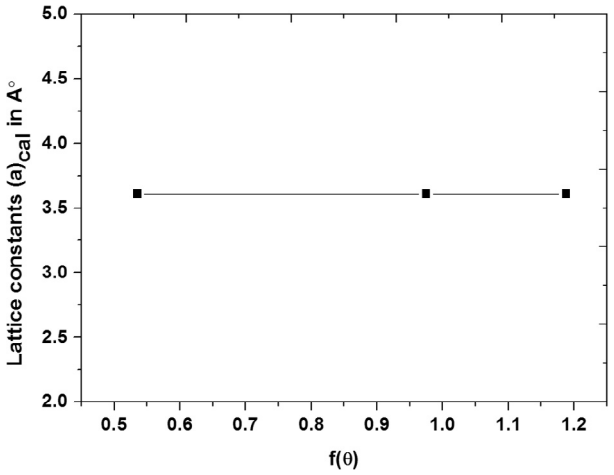

Figure 2 Nelson–Riley plots of Cu nanoparticles.

distinct peaks are observed at 2θ values 43.37°, 50.50° and 74.21° corresponding to (1 1 1), (2 0 0) and (2 2 0) Miller indices [20]. It was observed that diffraction peaks correspond to JCPDS No: 04-0836 and reveal that particles were Face Centred Cubic (FCC) in structure [21]. The Cu powder was observed to be well crystallized due to the sharpness in the major peak (1 1 1). From Fig. 1 we observe that the plane (1 1 1) modifies marginally towards the higher diffraction angle (2θ) by a value of 0.09 when compared with bulk value (2θ = 43.295; JCPDS 04-0836) showing compressive stress. The plane spacing 'd' was calculated using Bragg's equation. The lattice constant 'a' for FCC was calculated form the equation

$$a = d(h^2 + k^2 + l^2)^{1/2} \tag{1}$$

The lattice constants 'a' was corrected from the Nelson–Riley (N–R) plot and the values are shown in Table 1. N–R curve was plotted between the calculated values of 'a' for different planes and error function [22]

$$f(\theta) = \frac{1}{2}\left(\frac{\cos^2\theta}{\sin\theta} + \frac{\cos^2\theta}{\theta}\right) \tag{2}$$

Graph was plotted for the calculated 'a' versus $f(\theta)$ for Cu nanoparticles. By extrapolating the function $f(\theta)$ to zero the corrected value of lattice constant 'a' was found. This change in lattice constant indicated that grains were strained which is shown in Fig. 2. The collective effect of crystallite size and lattice strain due to dislocation was cause for the peak broadening of the sample [23]. The average particle size was calculated by Debey–Scherrer's formula [24] and size of the particles was 26.51 nm.

$$D = \frac{0.9\lambda}{\beta\cos\theta} \tag{3}$$

where λ, β, and θ are the X-ray wavelength (1.54 Å), the full width at half maximum (FWHM) of the diffraction peak and Bragg's diffraction angle respectively. Dislocation density (δ) was calculated with the crystalline size. The cumulative dislocation density was 1.42×10^{16} Lines/m^2.

$$\delta = \frac{1}{D^2} \tag{4}$$

The lattice constant of the bulk value a_o of Cu is 3.615 Å (JCPDS: 04-0836). This showed that there was certain amount of strain in the sample. The stress in the sample was mainly due to thermal expansion and intrinsically due to many factors like orientation, grain strain and lattice constants [25]. The average stress grown in the sample was given by the relation [26].

$$S = \left[\frac{a_o - a}{a_o}\right]\frac{Y}{2\sigma} \tag{5}$$

where a_o and a are lattice parameters of the bulk and nanoparticles respectively. Y and σ are Young's modulus and Poisson's ratio of the bulk material respectively. The values of Y and r for Cu bulk material are 140 Gpa and 0.34 respectively. From Williamson–Hall (W–H) plot the value of strain $\varepsilon = (a_o - a)/a_o$ is obtained. The values are shown in Table 1.

Residual stress and grain cause the XRD broadening in the sample. Therefore the actual size of the particles obtained from Scherrer's equation might be different. Strain may be the result of stress within the crystal and broadening may be due to the non-uniform strain in the material. Both size and strain broadening exist at once then crystallite size and strain may be found

Table 2 Geometric parameters of Cu nanoparticles prepared at room temperature ('D' – crystallite/grain/particle size, UDM – uniform deformation method, SSP – size–strain plot, PA – particle analyzer, WH – Williamson–Hall).

Name	'D' (in nm) from				Strain from WH plot ($\varepsilon \times 10^{-3}$)	Strain from SSP method ($\varepsilon \times 10^{-3}$)
	Scherrer's formula	UDM method (W–H) plot	SSP method	PA		
Cu	26.51	24.76	23.63	28	0.265	0.535

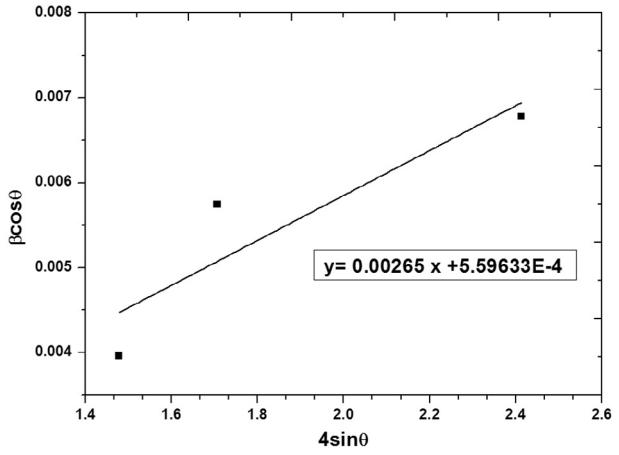

Figure 3 W–H plots of Cu nanoparticles.

from W–H plot [27]. Strain-induced broadening impending from crystal imperfections and distortion is related by $\varepsilon = \beta_s/4\tan\theta$. The size and strain broadening occur together from the total integral breath of Bragg peak [28]. We assume that both size and strain contribute to line broadening and they are independent of each other.

$$\beta_{hkl} = \beta_S + \beta_D \tag{6}$$

$$\beta_{hkl} = 4\varepsilon \tan\theta + \frac{K\lambda}{D\cos\theta} \tag{7}$$

Rearranging Eq. (7) we get

$$\beta_{hkl}\cos\theta = \frac{K\lambda}{D} + 4\varepsilon \sin\theta \tag{8}$$

The uniform deformation model (UDM) is represented in Eq. (7), where the strain is assumed to be uniform in all crystallographic directions. Thus considering the crystal as isotropic the materials properties are measure independent of the direction. The instrument's and sample dependent's effects are the cause of Bragg peak breath. To remove these aberrations, it is necessary to assemble a diffraction pattern from the line broadening of a standard material such as silicon to determine the instrumental broadening. The instrument-corrected broadening FWHM (β_{hkl}) is calculated using the following equation [29].

$$\beta_{hkl} = \left(\beta^2_{\text{measured}} - \beta^2_{\text{instrumental}}\right)^{1/2} \tag{9}$$

For all the three peak orientations we have plotted the graph with $\beta_{hkl}\cos\theta$ with respect to $4\sin\theta$. The crystallite size and strain ε are calculated from the y-intercept and the slope of linear fit respectively. The values are given in Table 2. From the W–H plot we consider that diffraction domain is isotropic and micro strain contribution is also considered. There is another method called 'size–strain plot' method to calculate the size–strain parameters for isotropic line broadening which is shown in Fig. 3. In this approach, the values at high angles are given less significance as their accuracy is less at those angles [30]. Using Lorentzian function the 'crystallite size' is calibrated and using Gaussian function strain is calculated [31]. We can write

$$\left(\frac{d_{hkl}\beta_{hkl}\cos\theta}{\lambda}\right)^2 = \frac{1}{D}\left(\frac{d^2_{hkl}\beta_{hkl}\cos\theta}{\lambda}\right) + \left(\frac{\varepsilon}{2}\right)^2 \tag{10}$$

The term $\left(\frac{d_{hkl}\beta_{hkl}\cos\theta}{\lambda}\right)^2$ is plotted against $\left(\frac{d^2_{hkl}\beta_{hkl}\cos\theta}{\lambda}\right)$ for the diffraction peaks of the sample. From linear fit data the crystallite size is calculated from the slope and the strain from y-intercept as shown in Fig. 4. The mean apparent size is $D_{\text{app}} = \frac{\lambda}{\text{slope}}$ and the actual size is obtained from $D = KD_{\text{app}}$ where $K = 3/4$ for spherical particle. The mean apparent strain is $\varepsilon_{\text{app}} = 2(\sqrt{y\ \text{intercept}})$ and the root square strain is obtained from $\varepsilon = \frac{\varepsilon_{\text{app}}}{2\pi\sqrt{2}}$ [32]. The assessed values of D and ε are tabulated in Table 2.

3.2. TG/DTA

Fig. 5 shows the TG curve of Cu powder. The total weight loss percentage of the sample is 3.328% shown in three stages. In the first stage the temperature range is 35–150 °C the weight loss is about 1.309% indicating the liberation of vapour in the sample. In the second stage the weight loss is 1.137% in the temperature range150–550 °C corresponding to the discharge of vapour from the interior pores of Cu. The third stage has a weight loss of 0.881% in the temperature range 550–800 °C showing dissipations of carbonaceous matter of

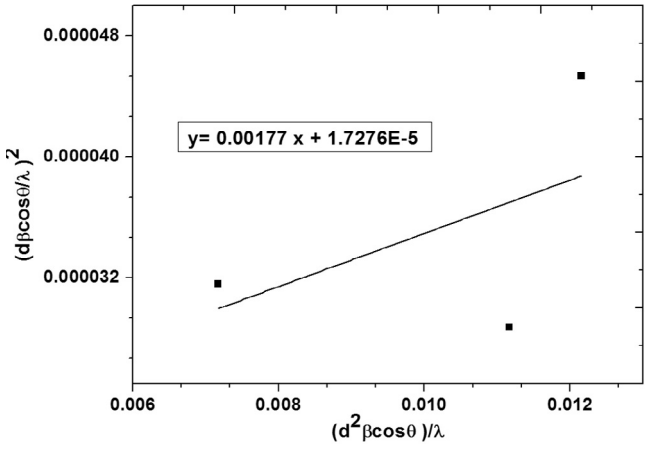

Figure 4 Size-strain plots of Cu nanoparticles.

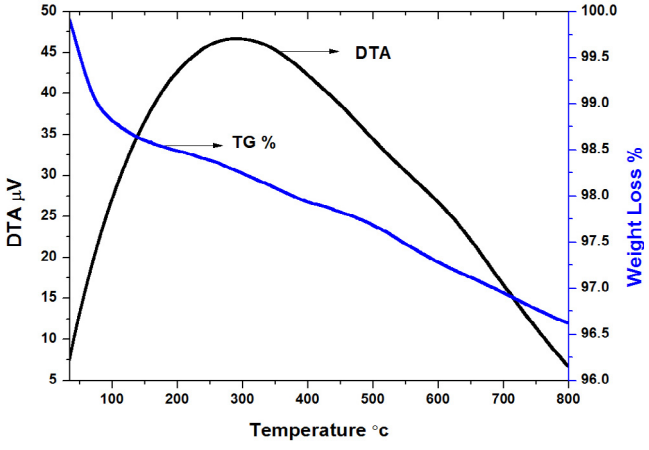

Figure 5 DTA/TG % curve of Cu nanoparticles.

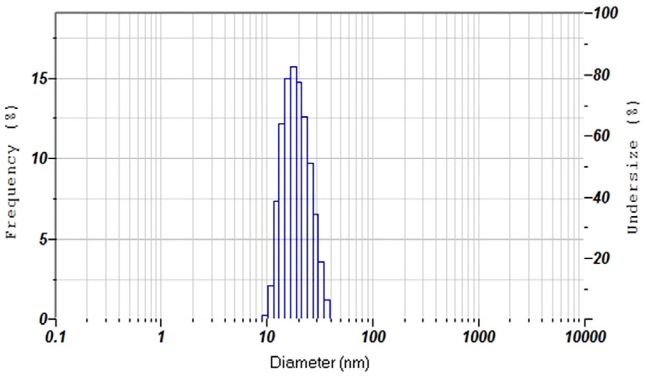

Figure 6 Particle size of Cu nanoparticles.

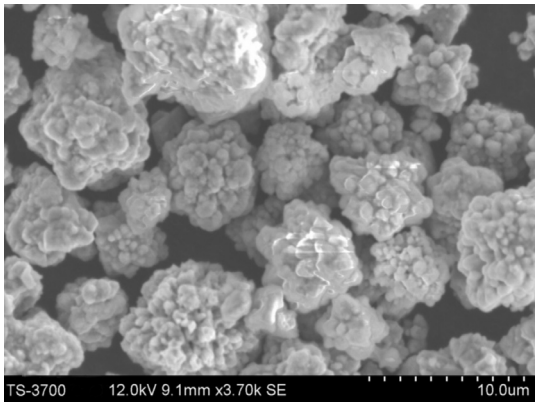

Figure 7 SEM micrograph of Cu nanoparticles.

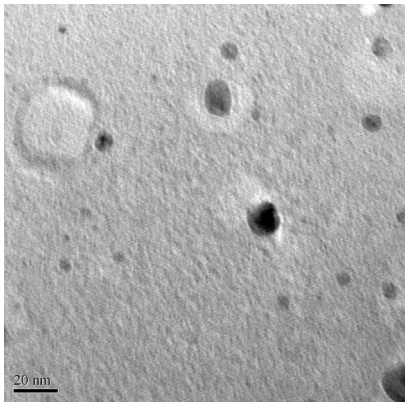

Figure 8 TEM image of Cu nanoparticles.

the sample. The weight loss is in very small percentage reflecting the purity of the sample. Due to slight existence of organic material in sample an exothermic peak at 290 °C was observed in DTA graph.

3.3. Particle analyser

Copper nanoparticles were ultra-stably suspended in the ethanol. The estimation of Cu particles in the suspension was calibrated using particle size analyser. In Fig. 6 particle size versus undersize percentage of histogram are shown. Under the dynamic light scattering, Cu particles showed the mean particle size as 28.9 nm. The crystallite size calculated from XRD, W–H and SSP is in good agreement with particle analyser.

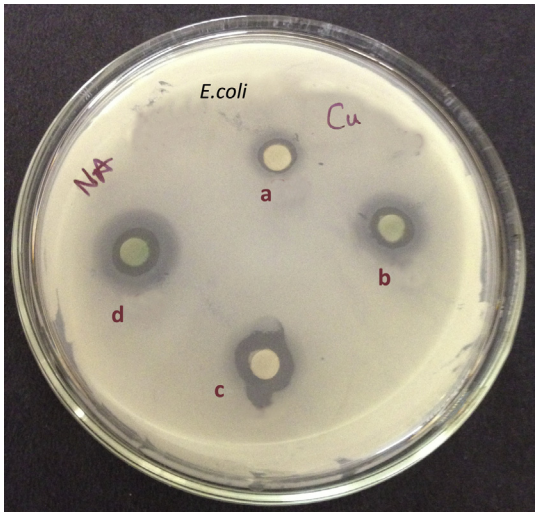

Figure 9 Antibacterial activity of Cu nanoparticles at different concentrations as a, b, c and d, against *E. coli*.

3.4. SEM

Examination of SEM micrographs revealed the shape and size. Fig. 7 shows the SEM image of copper nanoparticles. The morphology of copper nanoparticles was spherical and agglomerated.

3.5. TEM

From the TEM Fig. 8 it is revealed that the samples are with an average size of 20–25 nm which is in good agreement with that estimated by Scherer formula based on the XRD pattern.

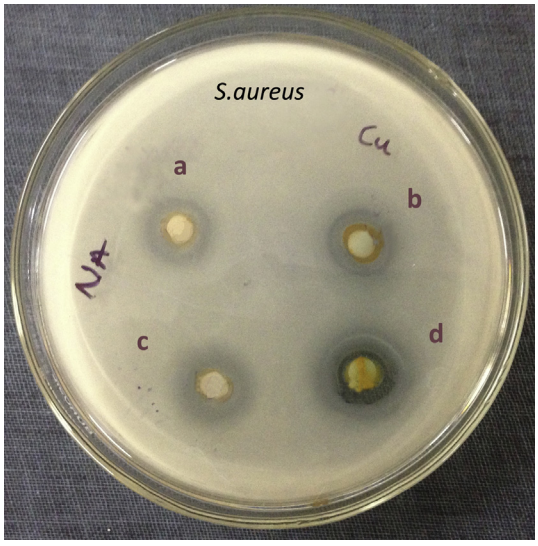

Figure 10 Antibacterial activity of Cu nanoparticles at different concentrations as a, b, c and d, against *S. aureus*.

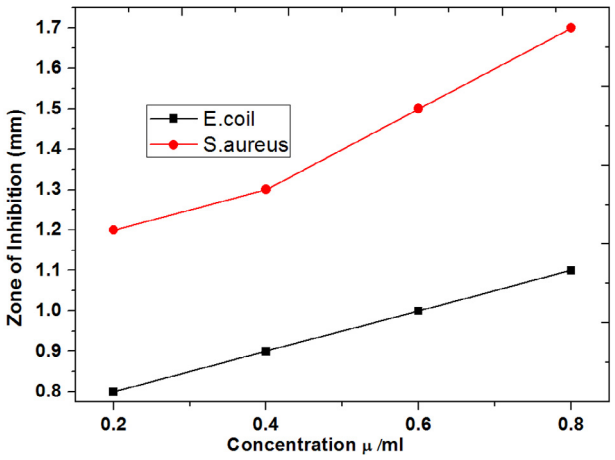

Figure 11 Zone of inhibition (mm) shown by Cu nanoparticles at different concentration.

3.6. Antibacterial activity

The effects of copper nanoparticles at different concentrations are shown in Figs. 9 and 10 at different concentrations like 0.2, 0.4, 0.6, 0.8 and1.0 μg/ml for different bacterial strains such as *E. coli* and *S. aureus*. As the concentration of copper nanoparticles was increased the inhibition zone measurements also showed increment which is shown in Fig. 11. It was observed that copper nanoparticles showed higher antibacterial activity for *S. aureus* than *E. coli* due to their thick cell wall with a number of mucopeptides and lipoteichoic acids (LTA) adding to this *S. aureus* has antioxidant enzyme which produces a stronger oxidant resistance [33]. *S. aureus* has very small negative charge when compared with *E. coli*. This would help *S. aureus* to permit more negative charged free radicals like superoxide ($-O^{-2}$) and hydroxyl radicals (–OH) to penetrate into the cell membrane and kill the cells [34]. Similar results in the antibacterial activity were observed for Fe_3O_4 nanoparticles on 4 bacterial strains [35]. Gram-negative bacteria are more sensitive when compared to Gram-positive bacteria. Earlier studies also indicate that gram-negative bacteria are less sensitive than gram-positive bacteria.

4. Conclusion

Copper nanoparticles are prepared by green synthesis method with Garcinia mangosteen leaves. The sample contains clusters of Cu nanoparticles. The sample is Face Centred cubic in structure which is revealed in XRD study. Peak broadening is observed due to small crystallite size and lattice strain. The line broadening is analysed by Scherrer formula, W–H plot and SSP methods. Particle analyser results are in good agreement with the results obtained by W–H plot and SSP methods. The results are in very close relation with one another. The weight loss percentage of the sample is 2.8385% which shows that the sample has high purity. Particle analyser reinforced the XRD calculations of crystallite size. SEM picture showed that particles were agglomerated. Antibacterial characterization against *E. coli* and *S. aureus* has showed that copper nanoparticles penetrated through the cell membrane resulting in inhibition zones.

References

[1] P. Mallick, C. Rath, R. Biswal, N.C. Mishra, Indian J. Phys. 83 (2009) 517.
[2] Y. Kayanuma, Phys. Rev. B Condens. Matter 38 (1988) 9797.
[3] M.P.C. Kalita, Mater. Lett. 87 (2012) 84.
[4] S.S. Nath, D. Chakdar, G. Gope, D.K. Avasthi, J. Nanotechnol. Online 4 (2008).
[5] G. Cao, Nanostructures and Nanomaterials, Imperial College Press, 2004.
[6] K. Chang, Tiny is Beautiful, Translating "Nano" into Practical, The New York Times, 2005.
[7] A.K. Schapter, H. Hu, A. Grenier, R. Schneider, F. Philips, Appl. Phys. A Mater. Sci. Process. 78 (2004) 73.
[8] R. Narayanan, ElM.A. El-Sayed, J. Am. Chem. Soc. 125 (2003) 8340.
[9] C. Li, Z. Liu, Y. Yang, Nanotechnology 17 (2006) 1851.
[10] S.P. Mondal, K. Das, A. Dhar, S.K. Ray, Nanotechnology 18 (2007) 95606.
[11] D. Mo, J. Liu, H.J. Yao, J.L. Duan, M.D. Hou, Y.M. Sun, Y.F. Chen, Z.H. Xue, L. Zhang, J. Crystal Growth 310 (2008) 612.
[12] J.S. Jang, U.A. Joshi, J.S. Lee, J. Phys. Chem. C 111 (2007) 13280.
[13] S. Kar, B.N. Pal, S. Chaudhuri, D. Chakravorty, J. Phys. Chem. B 110 (2006) 4605.
[14] Mohammad Mansoob Khan, Shafeer Kalathil, Jintae Lee, Moo Hwan Cho, Bull. Korean Chem. Soc. 33 (2012) 2592.
[15] Mohammad Mansoob Khan, Sajid Ali Ansari, Jin-Hyung Lee, M. Omaish Ansari, Jintae Lee, Moo Hwan Cho, J. Colloid Interface Sci. 431 (2014) 255.
[16] Bruna Lais Almeida Cunha, Jerônimo Pereira de França, Andrea Aparecida de Fátima Souza Moraes, Alba Lucilvânia Fonseca Chaves, Silvana Gaiba, Renato Fontana, Celio Kersul do Sacramento, Lydia Masako Ferreira, Lucimar Pereira de França, Acta Cir. Bras. 29 (2014) 2.
[17] P. Raveendran, J. Fu, S.L. Wallen, J. Am. Chem. Soc. 125 (2003) 13940.
[18] P. Selvakannan, S. Mandal, S. Phadtare, A. Gole, R. Pasricha, S.D. Adyanthaya, M. Sastry, J. Colloid Interface Sci. 269 (2004) 97.
[19] R. Haverkamp, A. Marshall, J. Nanopart. Res. 11 (2009) 1453.
[20] D. Mott, J. Galkowski, L.Y. Wang, J. Luo, C.J. Zhong, Langmuir 23 (2007) 5740.
[21] Ruimin Zhou, Xinfeng Wu, Xufeng Hao, Fei Zhou, Hongbin Li, Weihong Rao, Beam Interact. Mater. Atoms 266 (2008) 599.
[22] J.B. Nelson, D.P. Riley, An experimental investigation of extrapolation methods in the derivation of accurate unit-cell dimensions of crystals, Proc. Phys. Soc. London 57 (1975) 160.
[23] N. Choudhury, B.K. Sarma, Thin Solid Films 519 (2011) 2132.
[24] S. Sen, S.K. Halder, S.P. Sengupta, J. Phys. Soc. Jpn. 38 (1975) 1641.
[25] B. Barman, K.C. Sarma, Indian J. Phys. 86 (2012) 703.
[26] C.K. De, N.K. Misra, Indian J. Phys. 71 (1997) 535.
[27] P.K. Mochahari, K.C. Sarma, Indian J. Phys. 881265 (2014).
[28] Y.T. Prabhu, K. Venkateswara Rao, V. Sesha Sai Kumar, B. Siva Kumari, Int. J. Eng. Adv. Technol. 2 (4) (2013).
[29] K.D. Rogers, P. Daniels, Biomaterials 23 (2002) 2577.
[30] A.K. Zak, W.H.A. Majid, Ceram. Int. 36 (2010) 1905.
[31] M.A. Tagliente, M. Massaro, Phys. Res. B 266 (2008) 1055.
[32] P. Rageswari, S. Dhanuskodi, Cryst. Res. Technol. 48 (2013) 589.
[33] D. Wei, W. Sun, Q.W. Weiping, Y.Y. Yongzhong, M. Xiaoyuan, Carbohydr. Res. 344 (2009) 2375.
[34] Y.E. Lin, R.D. Vidic, J.E. Stout, C.A. Mccartney, V.L. Yu, Water Res 32 (1998) 1997.
[35] Y.T. Prabhu, K. VenkateswaraRao, B. Siva Kumari, Vemula SeshaSai Kumar, Pavani Tambur, Int. Nano Lett. 2 (2015).